

## FLOW OF VISCOPLASTIC LIQUIDS IN ROTATIONAL RHEOMETERS

Flávio H. Marchesini, fhmo@puc-rio.br  
Mônica F. Naccache, naccache@puc-rio.br  
Paulo R. de Souza Mendes, pmendes@puc-rio.br

Department of Mechanical Engineering  
Pontifícia Universidade Católica do Rio de Janeiro  
Rio de Janeiro, RJ 22453-900, Brasil

**Abstract.** *Viscoplastic liquids are found in several industries, from cosmetics to petroleum. This kind of fluid have very high viscosities at low stresses, and thin dramatically beyond a given threshold stress. Despite the increasing use of viscoplastic liquids, it is still very difficult to obtain an accurate rheological characterization. One of the main problems is apparent wall slip that can occur in the range of low and medium shear rates, leading to high experimental errors in viscosity data. In this work, some data using water-based carbopol dispersions are obtained experimentally using the rotational ARES rheometer (TA Instruments), with different geometries. A numerical solution was also performed to analyze the flow kinematics in these geometries, and to evaluate the assumptions used to obtain the experimental results. The solution of the conservation equations of mass and momentum were obtained via the finite volume technique using the FLUENT software. The Generalized Newtonian Fluid constitutive equation, and the SMD viscosity function (Souza Mendes and Dutra, 2004) were used to model the carbopol gel behavior. The experimental results for lower shear rates obtained with the smooth-Couette (bob-in-cup) and vane geometries were different from the ones obtained with the modified grooved-Couette. These results were compared to the numerical ones, and it was found a good agreement between the grooved geometry experimental data and the numerical simulations for smooth geometry with the no-slip condition at the wall, suggesting that wall slip took place in the experiments performed with smooth and vane geometries. Moreover, the numerical results showed that errors in experimental viscosity data could be obtained with vane and grooved geometries, due to flow kinematics pattern. Additionally, the numerically-obtained stress fields showed higher stress values near solid surfaces, both in grooved and vane geometries.*

**Keywords:** *rheometry, wall slip, viscoplastic liquids, carbopol dispersions*

### 1. INTRODUCTION

Structured fluids or yield stress materials are found in a wide variety of industries such as food, cosmetic, farmaceutical and petroleum. In these industries, knowing the accurately rheological properties of the viscoplastic fluid is fundamental for the success of many operations. Nevertheless, the rheometry of structured fluids still presents some challenges, such as yield stress measurements, apparent wall slip, thixotropy and the breakdown of structure on loading the material into the geometry used.

In experimental studies involving flows of viscoplastic liquids through different geometries it is frequently necessary to use a yield-stress fluid model (Curran et al., 2002). A good fluid model for its purpose needs to be transparent, inexpensive, and relatively easy to prepare and to modify its rheological properties. Among many thickeners that can be found, Carbopol is one of the most popular due to its characteristics (Piau, 2007). Carbopol gels behave like a viscoplastic liquid and can be considered a two-phase dispersion of swollen micro-gel particles in water (Taylor and Bagley, 1974).

One of the main problems in the rheometry of this kind of fluid is the presence of apparent wall slip during measurements. Apparent slip, or wall depletion effects, can occur in flows of structured fluids. It consists in a displacement of the disperse phase away from the solid boundaries, leaving a lower-viscosity, depleted layer of fluid adjacent to the wall. This lower-viscosity depleted layer makes easier the flow over the boundary, due to lubrication effect. This phenomenon is observed mainly in flows of structured fluids with low shear rates, large components as the disperse phase, smooth walls and small dimensions. In general, wall slip occurs in such a way that the apparent viscosity measured with different size geometries is not equal, and lower viscosities are obtained with smaller geometries. In addition, an apparent yield stress at lower stresses and sudden breaks in the flow curve can also be observed (Barnes, 1995).

The apparent slip of structured fluids can be characterized by obtaining enough data with different size geometries and then by doing a number of mathematical manipulations so as to end up with the bulk flow properties. On the other hand, as an attempt to eliminate wall slip during measurements and characterize the bulk fluid, several new rheometer geometries have been proposed by altering the physical or chemical character of the walls (Barnes, 1995). A common artifact to avoid wall depletion effects is to rough the surface (this is used in plate-plate and bob-in-cup geometries), which breaks the depleted layer of fluid if this layer is very thin. Other alternative is the vane geometry, a central shaft with a small number of thin blades arranged around at equal angles. The vane geometry, first exploited by Nguyen and

Boger (1983 and 1985) to measure the yield stress of concentrated suspensions has become a popular tool to characterize yield stress materials since then (Barnes and Carnali, 1990; Liddell and Boger, 1996; Barnes and Nguyen, 2001; Stokes and Telford 2004). The vane method consists in substituting the inner cylinder by the vane and assuming that the stress is uniformly distributed on a cylindrical sheared surface around the blades, to calculate the yield stress from the maximum torque (Nguyen and Boger, 1983 and 1985). Another consideration often used is that the apparent slip occurs only at the inner cylinder. It is based on Buscall et al. (1993), who found no slip at the outer cylinder for weakly attracted particle dispersions. However, Barnes (2000) proposed the addition of a slender gauze basket inserted inside an outer cylinder, so as to eliminate slip at the outer smooth wall, since slip can be found in rheological measurements of other structured fluids with simple vane geometry.

In this work, the traditional smooth-Couette (bob-in-cup), the simple vane and a modified grooved-Couette are analyzed experimentally and numerically so as to evaluate their performance in the rheometry of viscoplastic liquids. The modified grooved-Couette geometry consists in a bob-in-cup with vertical grooves both on the inner and on the outer cylinder. It follows the same idea of the vane and was employed to decrease the contact region between solid walls and fluid, avoiding the depletion phenomena. As a viscoplastic liquid model, aqueous carbopol dispersions are used.

## 2. EXPERIMENTAL STUDY

The experimental analysis was done using the rotational rheometer ARES (TA Instruments), and three different geometries, shown in Fig. 1:

- The original smooth-Couette geometry (two concentric cylinders with smooth walls);
- The simple vane geometry (one outer cylinder with smooth wall and one bladed cylinder);
- The grooved-Couette geometry (two concentric cylinders with grooved walls).

Although the concept of the use of two concentric cylinders for measuring the shear viscosity of liquids goes back to Stokes and Margules (Dontula et al., 2005), the development of this geometry for its purpose is attributed to Maurice Couette (Couette, 1888) since he was the first to control this apparatus (Piau and Piau, 2005). The measurements of the rheological properties in rotational rheometers are done applying a rotation in one of the cylinders and measuring the resulting torque. A scheme of the bob-in-cup geometry is shown in Fig. 2. The measured torque  $T$ , and rotation  $\Omega$  can be given at the inner or outer cylinder, depending on the rheometer manufacturer. The following hypotheses are considered: steady and laminar flow, axisymmetric flow, neglect end and gravity effects. Therefore, the flow is considered azimuthal ( $v_\theta = \Omega r$ ;  $v_r = v_z = 0$ ).



Figure 1. The geometries.

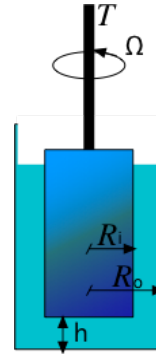


Figure 2. Scheme of bob and cup geometry

In the instrument used in our experiments, the torque  $T$  is measured at the inner cylinder. It is related to the wall shear stress by:

$$T = R_i \times F = R_i \times (\tau 2\pi R_i L) \Rightarrow \tau = \frac{T}{2\pi R_i^2 L} \quad (1)$$

where  $F$  is the shear force at cylinder wall and  $L$  is the cylinder length. The wall shear rate  $\dot{\gamma}$  is related to the rotational velocity (for  $R_i/R_o \neq 1$ ) by:

$$\dot{\gamma} = \frac{\Delta v}{\Delta r} = \frac{\Omega R_o}{R_o - R_i} \quad (2)$$

where  $\Delta v$  is the velocity variation between the two cylinders, and  $\Omega$  is the rotation velocity of the outer cylinder. Therefore, the viscosity at the cylinder wall is determined by:

$$\eta(R_i) = \frac{\tau(R_i)}{\dot{\gamma}(R_i)} = \frac{T/(2\pi R_i^2 L)}{\Omega R_o/(R_o - R_i)} \Rightarrow \eta(R_i) = \frac{T(1 - R_i/R_o)}{2\pi R_i^2 L \Omega} \quad (3)$$

The viscosity using the vane and grooved geometries is also determined by the above equations. In these cases, a hypothesis that the flow kinematics is similar to the one that occurs in the smooth-Couette geometry is done, considering that the fluid between blades/grooves moves together with the solid surfaces.

### 3. NUMERICAL ANALYSIS

#### 3.1. Mathematical modelling

The fluid is assumed to be homogeneous and incompressible. The flow under analysis is bi-dimensional, laminar and steady. The conservation equations of mass and momentum are given by:

$$\frac{\partial \rho}{\partial t} + \nabla \cdot \rho \mathbf{v}_r = 0 \quad (4)$$

$$\frac{\partial(\rho \mathbf{v})}{\partial t} + \nabla \cdot (\rho \mathbf{v}_r \mathbf{v}) + \rho(\boldsymbol{\omega} \times \mathbf{v}) = -\nabla p + \nabla \boldsymbol{\tau} + \rho \mathbf{g} \quad (5)$$

where  $\rho$  is the density,  $\mathbf{v}_r = \mathbf{v} - (\boldsymbol{\omega} \times \mathbf{r})$  is the relative velocity vector,  $\mathbf{v}$  is the velocity vector,  $\boldsymbol{\omega}$  is the angular velocity,  $p$  is the pressure,  $\mathbf{g}$  is the gravity acceleration, and  $\boldsymbol{\tau} = 2\eta \mathbf{D}$  is the extra-stress tensor.  $\mathbf{D} = 1/2(\nabla \mathbf{v} + \nabla \mathbf{v}^T)$  is the strain rate tensor, and  $\eta$  is the viscosity function, given by the SMD equation (Souza Mendes and Dutra, 2004):

$$\eta = (1 - \exp(-\eta_0 \dot{\gamma} / \tau_0)) (\tau_0 / \dot{\gamma} + K \dot{\gamma}^{n-1}) \quad (6)$$

In this equation,  $\dot{\gamma}$  is the shear rate, while  $\eta_0$ ,  $\tau_0$ ,  $K$ , and  $n$ , are respectively the low shear rate viscosity, the yield stress, the consistency index, and the behavior or power-law index. The physical meaning of these material parameters is discussed in detail by Souza Mendes and Dutra (Souza Mendes and Dutra, 2004).

In all three geometries analyzed, the smooth-Couette, the simple vane and the grooved-Couette, a torque  $T$  is applied at the central axis and the no-slip boundary condition is defined at walls. The inner cylinder is stagnant, and the outer cylinder rotates with an angular velocity equal to  $\Omega$ .

#### 3.2. Numerical solution

The governing conservation equations of mass and momentum were discretized using the finite volume technique. The commercial software FLUENT was used in the numerical simulations. Two different models were used to take into account the cylinder rotation. For the smooth-Couette and vane geometries, the Single Rotating Reference Frame (SRF) model (Fluent User's Guide, 2008) was employed, and the conservation equations (4) and (5) are solved at the entire computational domain. For the grooved geometry, the Multiple Rotating Reference Frame (MRF) model (Fluent User's Guide, 2008) was used. In this case, part of the domain is solved using the moving reference frame equations (eqs. (4) and (5)), and part considering stationary reference frame (i.e.,  $\omega=0$ ). At the interface between the two zones, a local reference frame transformation is performed so that variables in one zone can be used to calculate fluxes at the boundary of the adjacent zone (Fluent Users Guide, 2008).

The three geometries defined in the simulations were exactly the ones used in the experiments (shown in Fig. 1), except for the fact that in the numerical simulations, a bi-dimensional approach is used, neglecting end effects. The inner/outer diameters, as well as the meshes used are depicted in Table 1. The number of cells was chosen considering similar meshes in the annular space between cylinders. The Vane geometry is a six-blades geometry, and the vanes are 9.65 mm deep and 2 mm wide. In the Grooved geometry, the grooves are 1mm deep and 2mm wide, and are roughly 2 mm spaced.

Table 1. Geometry and Meshes

Geometry	Number of cells	Inner/outer diameter (mm)
Smooth-Couette	28800	32/34
Vane	56160	32/34
Grooved-Couette	130320	32/34

## 4. RESULTS AND DISCUSSION

### 4.1. Experimental Results

The experimental results were obtained with the ARES rotational rheometer, for a Carbopol dispersion in water, with 0,17 % concentration and pH=7. The experiments were performed using the three geometries described above, the bob-in-cup, the vane and the grooved. In this rheometer, the outer wall rotates and the inner wall is fixed. Figure 3 shows the viscosity obtained for the Carbopol dispersion. It can be observed that different results are obtained with the bob-in-cup and vane geometries, and the grooved one. For low shear rates or stresses, the bob-in-cup and vane geometries give lower values of viscosities, suggesting that wall slip occurred for shear stresses lower than 105 Pa. Moreover, it can be noted that since the result was the same for those geometries, slip seems to occur mainly at the outer wall. The Carbopol yield stress was evaluated using the flow curve obtained with the grooved geometry, shown in Fig. 4. All rheological parameters for the SMD viscosity function, eq. (6), were obtained via curve fitting, also using the grooved geometry result. Therefore,  $\tau_0=77.36$  Pa,  $\eta_0=1.67 \times 10^6$  Pa.s,  $K=24.46$  Pa.s<sup>n</sup>, and  $n=0.37$ .

The slip velocity was estimated using the experimental results, and is shown in Fig. 5. The outer wall velocity ( $v_{ns}$ ) was estimated using the grooved geometry and eq. (2), and is given by:

$$v_{so} = (\dot{\gamma}_{Va} - \dot{\gamma}_{Gr}) * (R_o - R_i) \quad (7)$$

where  $\dot{\gamma}_{Va}$  and  $\dot{\gamma}_{Gr}$  are the shear rates measured by the rheometer, using the vane and grooved geometries respectively. This equation considers that the excess on shear rate measured with the vane geometry is due to apparent slip. The inner wall slip velocity was obtained using the bob-in-cup geometry, assuming that the excess on shear rate values, compared to the ones measured with the vane geometry, is due to inner wall slip (i.e., outer wall slip was admitted to be the same with the vane and the bob-in-cup geometries). Then, the inner wall slip velocity is estimated by:

$$v_{si} = \left[ \dot{\gamma}_{BC} - \dot{\gamma}_{Gr} - \frac{v_{so}}{(R_o - R_i)} \right] * (R_o - R_i) \quad (8)$$

With the aid of Fig. 5, it can be noted that at lower stress, outer wall slip is higher than inner wall slip. As the shear stress increases, the inner and outer wall slip tend to the same value.

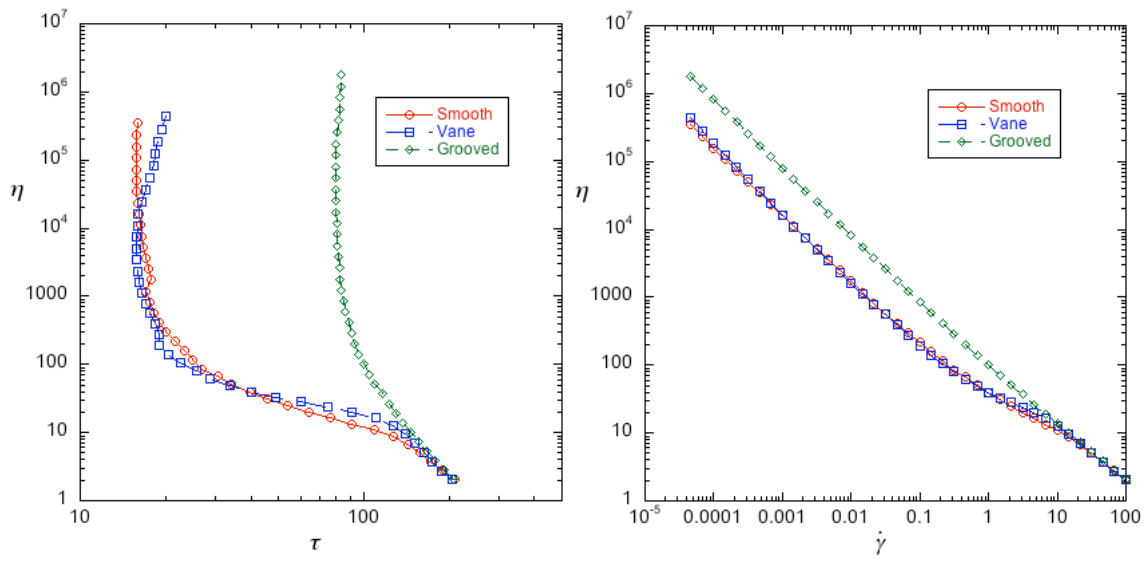


Figure 3. Viscosity of Carbopol dispersion 0,17%, as a function of (a) shear stress, and (b) shear rate.

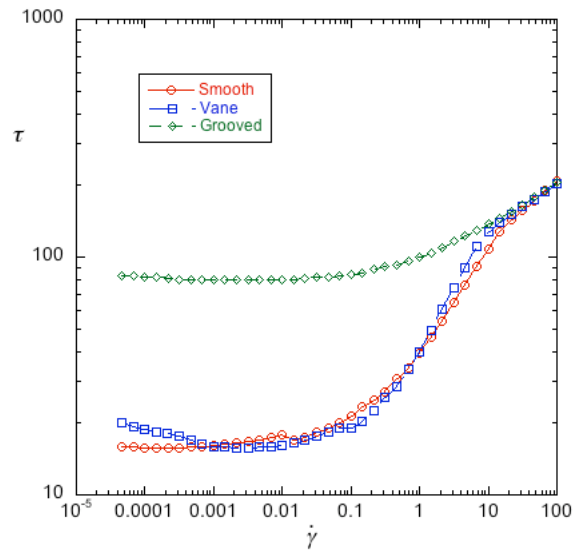


Figure 4. Flow curve of Carbopol dispersion 0,17%.

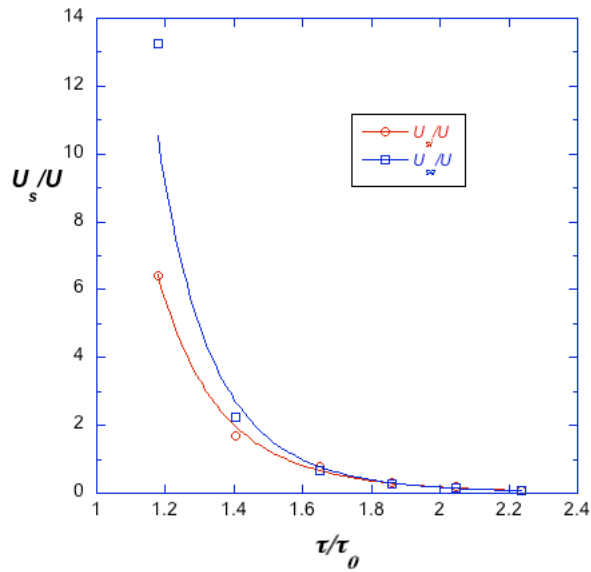


Figure 5. Inner and Outer wall slip velocities.

#### 4.2. Numerical Results

Figures 6-11 show the velocity and strain rate pattern for the three different geometries and two different experimental shear rate values. The dimensionless shear rate is defined using the characteristic shear rate  $\dot{\gamma}_1 = (\tau_0 / K)^{1/n}$ . In the bob-in-cup geometry it is noted that shear rates (and shear stresses) are higher at the outer wall, as expected. The results for the vane geometry, presented in Figs. 8 and 9, show that a stress concentration occurs at the blades extremity. Moreover, it is observed that the fluid invades the space between blades, and the flow pattern deviates from that observed in the bob-in-cup geometry. As the rotation is increased, the invasion is even more critical. Figures 10 and 11 show the results for the grooved geometry. It is observed that fluid invasion occurs as well, but it can be pointed out that the kinematics deviation from the bob-in-cup behavior is more critical in the vane.

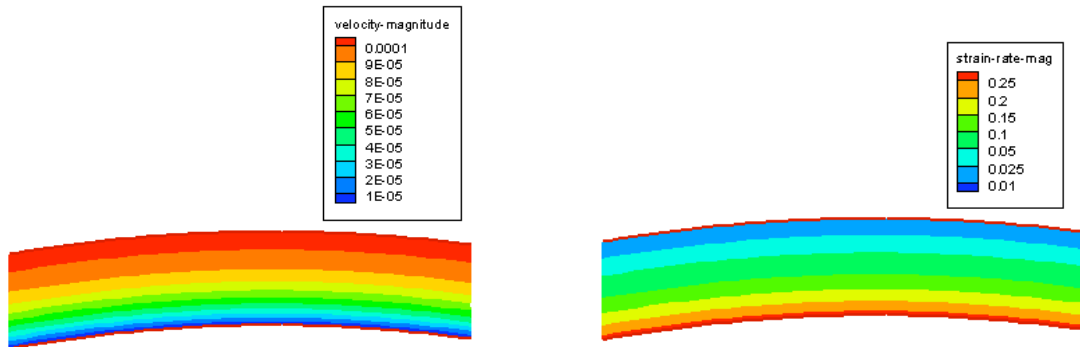


Figure 6. Velocity and strain rate for bob and cup geometry, and  $\dot{\gamma}_{\text{exp}} / \dot{\gamma}_1 = 4.4 \times 10^{-3}$

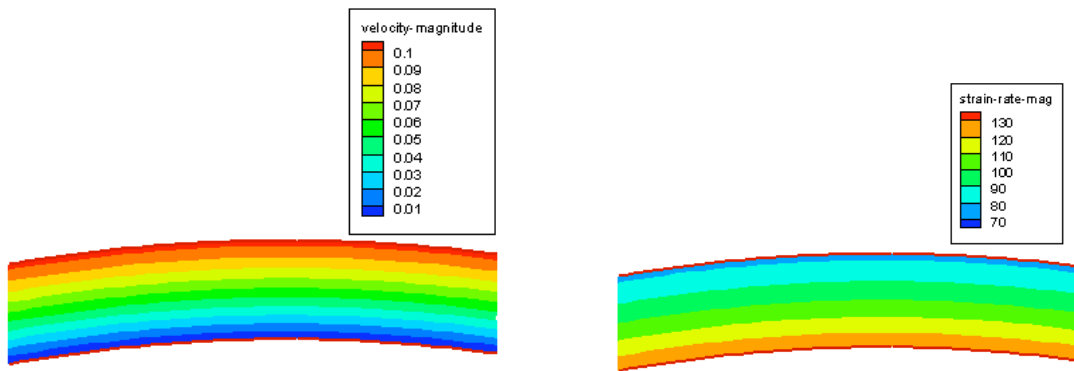


Figure 7. Velocity and strain rate for bob and cup geometry, and  $\dot{\gamma}_{\text{exp}} / \dot{\gamma}_1 = 4.4$

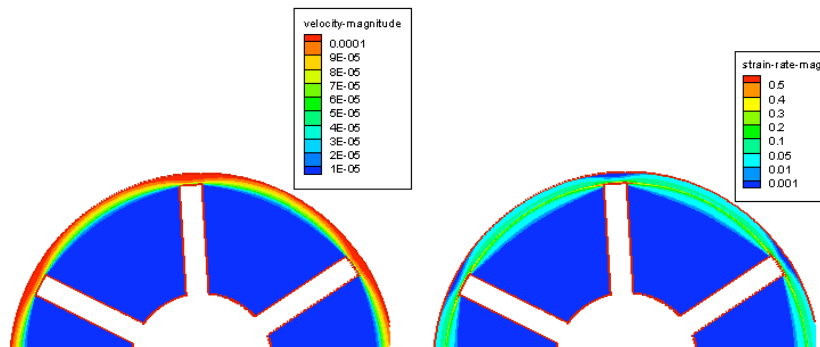


Figure 8. Velocity and strain rate for the vane geometry, and  $\dot{\gamma}_{\text{exp}} / \dot{\gamma}_1 = 4.4 \times 10^{-3}$

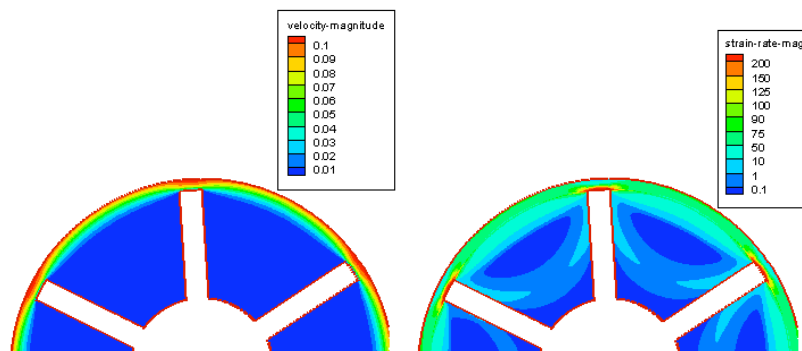


Figure 9. Velocity and strain rate for the vane geometry, and  $\dot{\gamma}_{\text{exp}} / \dot{\gamma}_1 = 4.4$

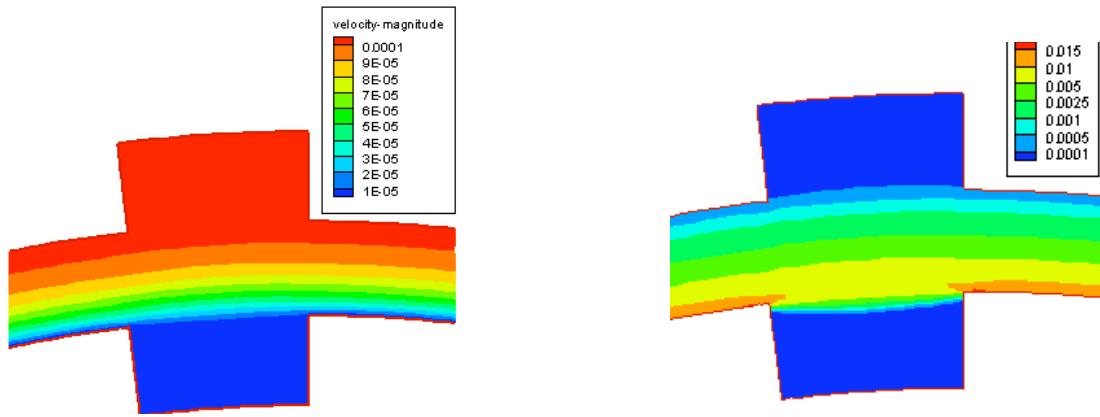


Figure 10. Velocity and strain rate for the grooved geometry, and  $\dot{\gamma}_{\text{exp}} / \dot{\gamma}_1 = 4.4 \times 10^{-3}$

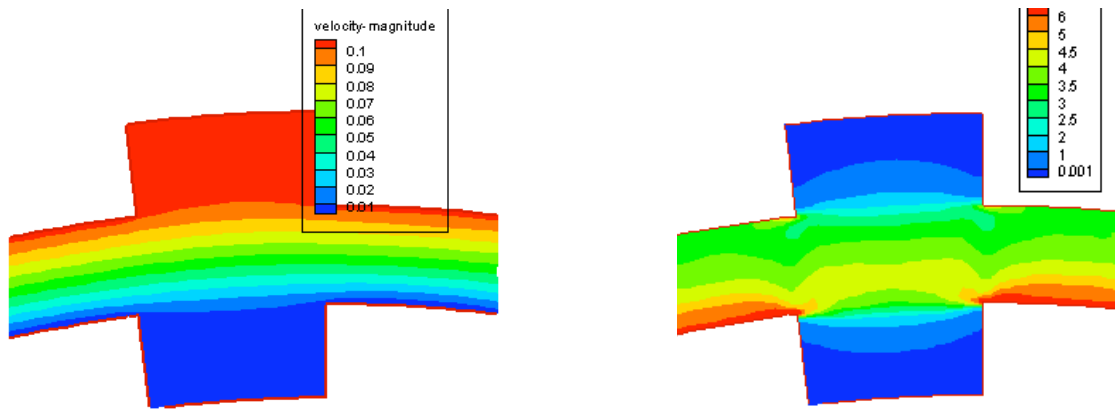


Figure 11. Velocity and strain rate for the grooved geometry, and  $\dot{\gamma}_{\text{exp}} / \dot{\gamma}_1 = 4.4$

Figure 12 shows the dimensionless velocity ( $v_R = \Omega R_0$ ) and shear rate profiles for the three geometries with outer wall dimensionless shear rate equal to  $4.4 \times 10^{-3}$  and 4.4. It can be observed that for lower shear rates (lower rotations) the velocity profile is highly non-linear, which could lead to high errors in the experimental viscosity evaluation (see eqs. (2) and (3)). It is also observed that the grooved and bob-in-cup profiles are similar at this range of rotation, showing that the grooved flow pattern in the annular space can be considered similar to the one in the bob-in-cup geometry.

Figure 13 shows the inner and outer wall shear stress as a function of the imposed shear rate. It is noted that outer wall shear stresses are lower than the inner ones. The outer wall shear stress is equal for the vane and bob-in-cup geometries. At the inner wall, the grooved and vane shear stress deviate from the bob-in-cup one, due to flow kinematics.

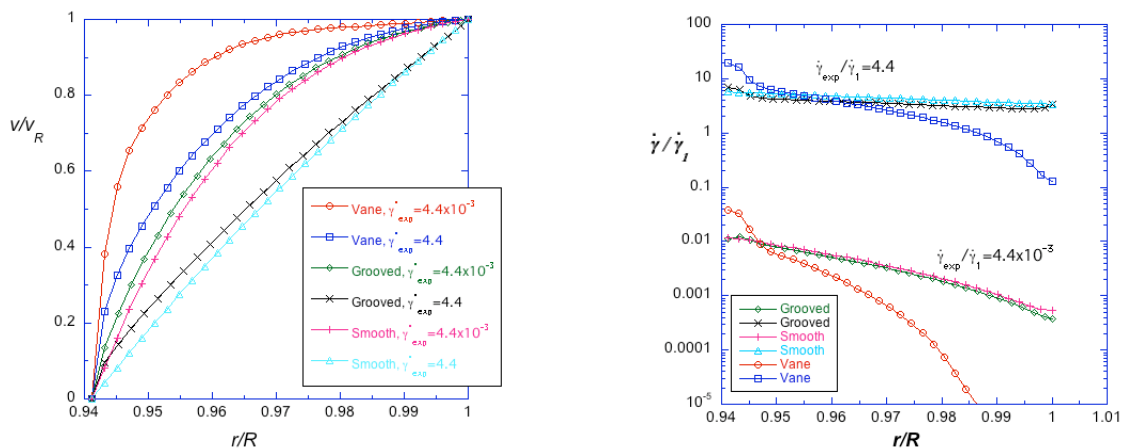


Figure 12. (a) Velocity profiles and (b) strain rate profile for the three geometries and dimensionless experimental outer wall shear rate equal to  $4.4 \times 10^{-3}$  and 4.4.

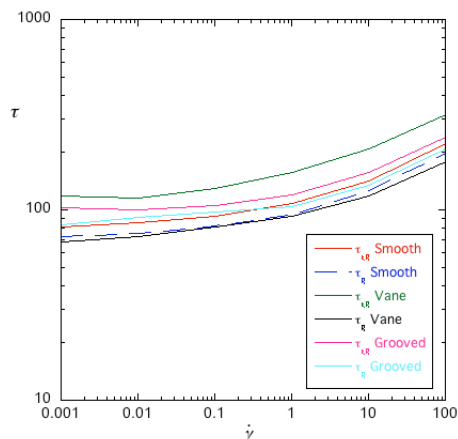


Figure 13. Inner and outer wall shear stress for the three geometries.

### 4.3. Comparison between Computation and Experiments

A comparison between numerical and experimental results is shown in Fig. 14. It is observed that the inner wall shear stress obtained experimentally with the grooved geometry, is similar to the numerical bob-in-cup geometry, showing that no slip is occurring in the experiments with this geometry. However, both bob-in-cup and vane experimental results show that wall slip is occurring.

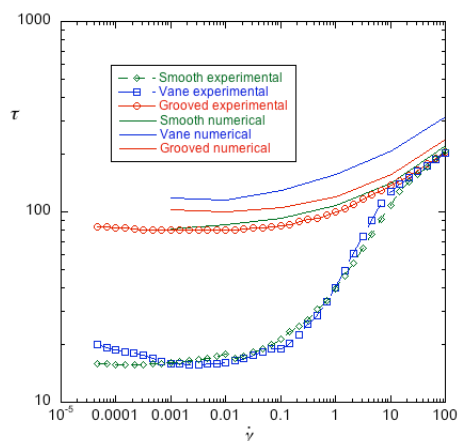


Figure 14. Comparison of inner wall shear stress between experimental and numerical results

## 5. FINAL REMARKS

In this work, a numerical and experimental analysis was performed to analyze apparent wall slip in viscosity measurements of viscoplastic liquids in rotational rheometers. Three different geometries were used in the experiments: the bob-in-cup, the vane and the grooved. The numerical simulation was performed using the finite volume technique and the Fluent software. It was observed that for viscoplastic liquids, wall slip occurs mainly at lower shear stresses. At this range, the outer wall slip velocity is much higher than the inner one for the carbopol dispersion studied, contradicting Buscall et al. (Buscall et al., 1993) who found no slip at the outer cylinder wall for weakly attracted particle dispersions. At higher shear stresses, no slip was detected, and all geometries perform well. It was also shown that flow kinematics is affected in the vane and grooved geometries, which could lead to experimental errors in the viscosity measurements. At last it is important to point out that the grooved geometry performance was better than the other ones in the rheological measurements realized, but more investigation is necessary.

## 6. ACKNOWLEDGEMENTS

The authors are indebted to Petrobras S.A., CNPq, CAPES, FAPERJ, FINEP, and MCT for the financial support to the Group of Rheology at PUC-RIO.

## 7. REFERENCES

- H. A. Barnes, *J. Non-Newtonian Fluid Mech.* 56, 221–251 (1995).
- H. A. Barnes, *A handbook of elementary rheology*, University of Wales, (2000).
- H. A. Barnes, and J. O. Carnali, *J. Rheol.* 34(6), 841–866 (1990).
- H. A. Barnes, and Q. D. Nguyen, *J. Non-Newtonian Fluid Mech.* 98, 1–14 (2001).
- R. Buscall, J. I. McGowan, and A. J. Morton-Jones, *J. Rheol.* 37(4), 621–641 (1993).
- M. Couette, *Compt. Rend.* 107, 338-390 (1888).
- S. J. Curran, R. E. Hayes, A. Afacan, M. C. Williams, and P. A. Tanguy, *J. Food Sci.* 67(1), 176-180 (2002).
- P. Dontula, C. W. Macosko, and L. E. Scriven, *J. Rheol.* 49, 1551–1551 (2005).
- Fluent Users Guide, (2008).
- P. V. Liddell, and D. V. Boger, *J. Non-Newtonian Fluid Mech.* 63, 235-261 (1996).
- Q. D. Nguyen, and D. V. Boger, *J. Rheol.* 27(4), 321-349 (1983).
- Q. D. Nguyen, and D. V. Boger, *J. Rheol.* 29(3), 335-347 (1985).
- J. M. Piau, and M. Piau, *J. Rheol.* 49, 1539–1550 (2005).
- J. M. Piau, *J. Non-Newtonian Fluid Mech.* 144, 1–29 (2007).
- P. R. Souza Mendes, and E. S. S. Dutra, *Appl. Rheol.* 14, 296–302 (2004).
- J. Stokes, and J. Telford, *J. Non-Newtonian Fluid Mech.* 124, 137–146 (2004).
- N. W. Taylor, and B. Bagley, *J. Appl. Polym. Sci.* 18, 2747-2761 (1974).

## 8. RESPONSIBILITY NOTICE

The authors are the only responsible for the printed material included in this paper.